Kinetic critical temperature and optimized chemical vapor deposition growth of carbon nanotubes

Vinten, P.; Lefebvre, J.; Finnie, P.

Publisher's version / Version de l'éditeur:
https://doi.org/10.1016/j.cplett.2008.12.095
Chemical Physics Letters, 469, 4-6, pp. 293-297, 2009-01-03

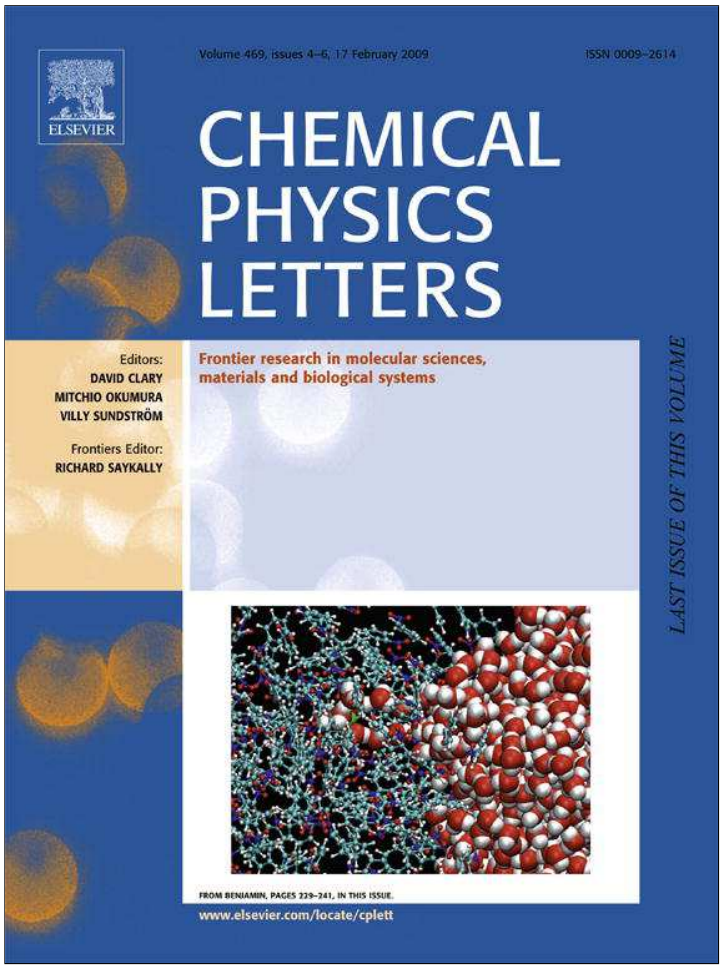

Chemical Physics Letters 469 (2009) 293–297

Contents lists available at ScienceDirect

Chemical Physics Letters

journal homepage: www.elsevier.com/locate/cplett

Kinetic critical temperature and optimized chemical vapor deposition growth of carbon nanotubes

P. Vinten [a,b], J. Lefebvre [a], P. Finnie [a,b,*]

[a] Institute for Microstructural Sciences, National Research Council Canada, Building M-50, 1200 Montreal Road, Ottawa, ON, Canada K1A 0R6
[b] Department of Physics, University of Ottawa, 150 Louis Pasteur, Ottawa, ON, Canada K1N 6N5

ARTICLE INFO

Article history:
Received 18 September 2008
In final form 23 December 2008
Available online 3 January 2009

ABSTRACT

The existence of a critical temperature T_c in the chemical vapor deposition growth of carbon nanotubes, including single-walled nanotubes, is shown by *in situ* optical imaging of growing nanotube forests. At T_c, the temperature dependence of the chemical processes and characteristics of the grown nanotubes change. The lifetime and initial growth rate show this critical temperature and are linked by a characteristic energy through the initial growth rate decay. *Ex situ* Raman spectroscopy shows that the number of radial breathing modes, G band, and D band show the same characteristic energies and T_c.

1. Introduction

Chemical vapor deposition (CVD) is a leading approach for the synthesis of carbon nanotubes, with single-walled nanotubes (SWNTs) being routinely synthesized in high yield using many source gases and types of catalyst [1]. Still, the CVD microscopic growth process is only understood in broad terms. The underlying critical physical and chemical steps have yet to be clearly identified. This is a barrier toward rational synthesis of SWNTs. *In situ* studies are promising for improving our understanding of the growth process. Nanotube forests (close packed vertically aligned arrays) are particularly useful for *in situ* studies of growth dynamics [2–8] due to their macroscopic size. Forests have been grown by CVD for over a decade [9,10] and have more recently been grown with large fractions of SWNTs [4,11–13]. Here, we use *in situ* optical imaging of growing forests [5,14,15] to show the existence of a critical point for thermal CVD that is kinetic in origin. The critical point appears in the temperature dependence, at a critical temperature T_c, of the initial growth rate β and the lifetime τ. The initial growth rate and the lifetime are linked by a characteristic energy through the initial growth rate decay β/τ. This suggests that the origin of their scaling is a single molecular process. *Ex situ* Raman spectral properties and the abundance of SWNTs also show this critical point, which provides a link to the kinetic parameters. We attribute the critical point to the optimum feeding of the system with carbon source gas, which has direct consequences on the growth dynamics and properties of the grown nanotubes.

2. Experiment

Nanotubes were grown in a cold wall CVD reactor similar to those described in previous reports [16,17]. Cold wall CVD reactors are well suited to optical monitoring because they allow excellent optical access to the sample [14,17,18]. Samples were $\sim 0.4\ cm^2$ square pieces of 0.5 mm thick Si with 1 μm SiO_2. Catalyst layers, nominally of 250 nm Al_2O_3 and 0.8 nm Co [19], were deposited by e-beam evaporation through a shadow mask to produce a regularly spaced pattern of 0.7 mm diameter circles. Samples were heated to the growth temperature T in pure carrier gas (98% Ar, 2% H_2) flowing at 260 sccm at atmospheric pressure. T was measured with a two color infrared pyrometer. Ethanol vapor was used as the carbon source [20] by diverting the carrier gas through a bubbler and delivering it to the sample through a narrow tube directed down at an angle of $\sim 45^\circ$. When no noticeable growth occurred for an ~5 min interval, the reactor was purged with pure carrier gas for several minutes before allowing it to cool. Forests were grown vertically and imaged *in situ* nearly edge on (~5°) using a long working distance optical microscope and digital camera. Videos were recorded for each growth run (see Supplementary material). Final height H_f was calibrated *ex situ* via scanning electron microscopy (SEM, Hitachi S-4700). SEM observation indicates that most nanotubes in the forest are aligned and reasonably straight, implying that the height of the forests is approximately the length of the individual nanotubes.

Raman spectra were obtained *ex situ* using a commercial confocal Raman system (Jobin Yvon Labram) with a 300 line/mm grating and 50X extra-long working distance microscope objective. We used 785 nm and 1 mW excitation on a spot of ~1 μm in diameter and a confocal hole of 100 μm. At this power density, there was no damage to the forests, however if the power was increased by even less than an order of magnitude, irreversible damage was done to

* Corresponding author. Address: Institute for Microstructural Sciences, National Research Council Canada, Building M-50, 1200 Montreal Road, Ottawa, ON, Canada K1A 0R6.
E-mail address: Paul.Finnie@nrc-cnrc.gc.ca (P. Finnie).

0009-2614/$ - see front matter
doi:10.1016/j.cplett.2008.12.095

the forests. The total laser exposure was identical for all points with a total of 9 s acquisition composed of three 3 s acquisitions at each data point. We scanned each sample across a 5×5 grid covering a 120 μm × 120 μm area. This was done twice for a total of 50 spectra per sample. The samples were analyzed from the tops of the forests (90° to the substrate), and the laser was linearly polarized parallel to the substrate surface (perpendicular to the average nanotube axis, which was vertical).

3. Results

Several video frames of a growth at 725 °C are shown in Fig. 1a. Fig. 1b shows the height of the forest H as a function of growth time t, extracted from the video with ~2 μm resolution. The line is a fit to the exponential decay model of [3]: $H(t) = \beta\tau(1 - e^{-t/\tau})$. Here, $H_f = H|_{t\to\infty} = \beta\tau$. The second time derivative (the time derivative of the growth rate) has β/τ as the exponential prefactor. In [3], this functional form of $H(t)$ was used for water assisted ethylene CVD. The same functional form has also been used to explain optical absorption data for ethanol CVD [7]. A low magnification SEM image, similar to those used to calibrate H_f, is shown in Fig. 1c. This model provided a good fit at all T. As verification, all of the height data was collapsed onto a single curve of normalized height vs normalized time (Fig. 1d) by dividing H by H_f and t by τ. For a perfect fit, all data would collapse on the red curve. All of our data is close to this single curve and we therefore conclude that the fit is indeed universal to a good approximation.

Fig. 2a shows a plot of H_f vs $1/k_BT$ where k_B is Boltzmann's constant. Forest heights of ~125 μm were typical for 675 °C < T < 870 °C. Below 675 °C, H_f dropped off rapidly. Above 870 °C, H_f decreases with increasing T, with a characteristic energy of -2.3 ± 0.3 eV. Note that the characteristic energy has a sign opposite to that of the slope. If a dataset Y fits a straight line on a $\ln Y$ vs $1/k_BT$ plot, we define the characteristic energy as the negative of the slope. Then, if the dataset Y is a reaction rate, the characteristic energy is positive and has the meaning of activation energy.

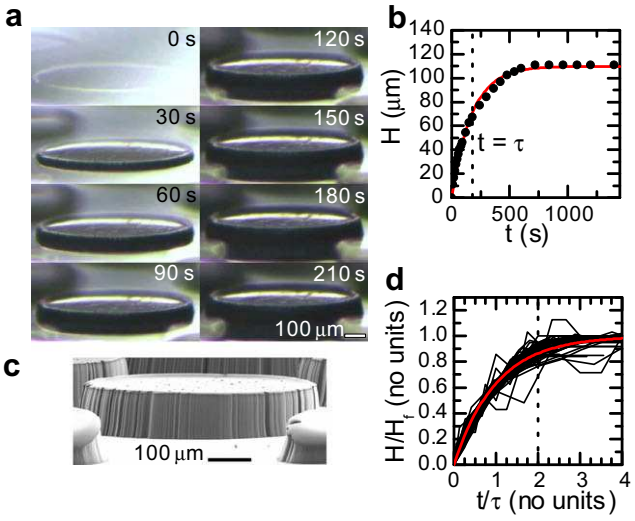

Fig. 1. (a) Video frames from a growth at 725 °C (see Supplementary material). Angle of inclination is ~ 5°. (b) Height H as a function of growth time t (points) and exponential decay fit (line). (c) Low magnification *ex situ* SEM image of the same forest at a similar angle. (d) In a plot of normalized height H/H_f vs normalized time t/τ, all data collapsed onto a single curve (red). The red line is the ideal situation, where $H_f = \tau = 1$. (For interpretation of the references to colour in this figure legend, the reader is referred to the web version of this article.)

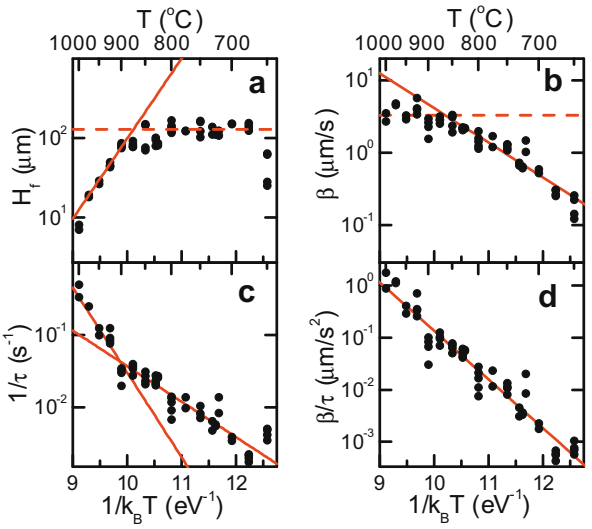

Fig. 2. Plots of kinetic parameters vs $1/k_BT$. (a) Final height H_f; (b) initial growth rate β; (c) inverse lifetime $1/\tau$; and (d) initial growth rate decay β/τ. All show the same functional form with characteristic energies. (a–c) show critical point. Solid lines are linear fits, dashed lines are to guide the eye.

Plots of β vs $1/k_BT$ and $1/\tau$ vs $1/k_BT$ (Fig. 2b and c, respectively) reveal simple linear scaling of both parameters, but with a change in slope at $T_c \approx 870$ °C. These two parameters are rates: the nanotube growth rate and the catalyst decay rate, respectively. It is reasonable to assume that these rates correspond to the rates of specific chemical steps. These plots are then Arrhenius plots and the characteristic energy has the meaning of activation energy. Above T_c, β is approximately constant at 3.3 ± 1.0 μm/s, and is therefore not limited by T. Below T_c, β is activated at 1.1 ± 0.1 eV, similar to previous reports for thermal CVD with other catalysts and source gases [6,7,21–24]. The lifetime τ also shows a change in temperature dependence at $T_c \approx 870$ °C. Above T_c, $1/\tau$ shows an activation energy of 2.4 ± 0.2 eV, a similar order of magnitude for iron catalyst and ethylene source gas [25]. Below T_c, $1/\tau$ shows an activation energy of 1.2 ± 0.1 eV, the same value within error as β (as expected the activation energies of β are simply the sums of the energies in H_f and $1/\tau$). Ref. [7] reported an activated β at the optimum pressure (we use a constant pressure), but observed a constant τ. This activated β is likely another manifestation of the critical point. The fact that β and τ have the same activation energy below T_c suggests that they are directly and causally linked by the same molecular process. This is the rate limiting step of the growth process, which may be, for example, the chemical decomposition of ethanol.

Further evidence for a single molecular process comes from a plot of the ratio β/τ vs $1/k_BT$ (Fig. 2d). This parameter β/τ represents the rate of the process that causes the growth to slow down exponentially. β/τ shows a characteristic energy of 2.4 ± 0.2 eV over the entire temperature range, with no evidence of a critical temperature. As expected, this energy is the sum of the activation energies of β and $1/\tau$, but importantly β/τ shows only one characteristic energy across the entire temperature range, which suggests it originates in a single molecular process. At high T, both τ and β/τ show, within error, the same high characteristic energy. This energy then represents a process that competes with growth and only occurs alongside growth. It acts at all T but only dominates above T_c. Interestingly, this energy is the same, within error, to the activation energy for defect diffusion, which has recently been determined to be ~2.2 eV [26]. We speculate that defect diffusion to the growth front is a possible explanation for the growth termination and the observed values of τ. Alternatively, others have

attributed the activation energy of τ to catalyst deactivation via interaction with the catalyst support [25].

Elementary considerations provide some insight into these characteristic energies. Kinetic limits can arise from processes at the single nanotube level or from the collective effects of many nanotubes. A collective process of interest is the degree to which diffusion through the forest limits growth [5,27–30]. Here, τ decreases even as H_f decreases (at high T), contrary to expectations if diffusion through the forest is important. Also, our forests have edges, so extreme edge effects would be expected if diffusion through the forest was important. However, these forests are relatively uniform in height. Therefore, growth limitations due to diffusion through the forest are neglected and we turn our attention to effects at the single nanotube level.

For a single nanotube, β can be estimated if we assume ethanol molecules behave like an ideal gas and are carried at equilibrium (partial pressure $P \approx 6$ kPa at room temperature) with the carrier gas to the reaction site. The molecular impingement rate on a nanoparticle of ~1–2 nm diameter is $\sim 4\text{—}20 \times 10^8$ s^{-1} (using flux $F = P(2\pi m k_B T)^{-1/2}$ where m is the mass). For a ~1–2 nm diameter SWNT, with carbon surface density $\sim 4 \times 10^{19}$ m^{-2}, this corresponds to $\beta \sim 1$–16 mm/s, much higher than observed. If there is an energy barrier to growth $E = 1.1$ eV that scales the impingement rate by a factor $e^{-E/k_B T}$, then (using $T = T_c$) $\beta \sim 0.015$–0.22 μm/s, a similar order of magnitude to the observed value. Conversely, considering the observed value of 3.3 μm/s at T_c, this impingement rate would correspond to an energy barrier of ~0.6–0.8 eV which is close to the observed value.

Raman spectroscopy provides further insight into the growth kinetics. Raw spectra in the SWNT radial breathing mode (RBM) region ($\omega \leqslant 300$ cm^{-1}) and D and G band regions are shown in Fig. 3a for several T. For all spectra (except 600 °C, which was not a vertically aligned forest but rather had only surface tubes) the focal depth of the laser was entirely within the forest because the Si peak around 500 cm^{-1} was completely absent from the spectra. The focal depth is therefore less than ~10 μm, the shortest forest analyzed (1000 °C).

Fig. 3b shows the D/G integrated intensity ratio I_D/I_G vs $1/k_B T$. This is a common measure of the quality of the sample. I_D/I_G as a function of T reaches a minimum, consistent with previous reports [6,27,31–33]. We identify this minimum at T_c and the characteristic energy gives it new meaning. I_D/I_G decreases with T with a characteristic energy of -1.1 ± 0.1 eV below T_c. Above T_c it increases with a characteristic energy of 1.1 ± 0.1 eV, the same value. The temperature dependence of I_D/I_G therefore contains information beyond sample quality. Very recently, *in situ* Raman spectral data with the ln $(I_D/I_G) \propto 1/k_B T$ functional form and characteristic energy has been presented and from it, an activated and critical β and τ were inferred [24]. The energy of 1.1 eV characterizes the limiting step in this chemical process as an activation energy in the Arrhenius plot of β, but also manifests itself in I_D/I_G. This suggests that the generation of non-sp^2 bonds, such as the build-up of amorphous carbon, vacancies, or other defects, is linked to the growth process. At T_c, we speculate that there is optimum feeding of carbon source gas and that any deviation from T_c will produce more defects, thus increase I_D/I_G.

The average number of RBMs per spot N (here we used 50 Raman spectra) is statistically meaningful and we find that it is a good metric for comparing samples [34]. Since the spot size is ~1 μm, N is effectively the surface density of resonant SWNTs (i.e.: SWNTs/μm^2). Forests of nanotubes are not especially dense, typically consisting of small bundles of several tubes spaced by, on the order of, 100 nm. A 1 μm diameter spot would then see on the order of 1000 nanotubes. Our samples have wide chirality and diameter distributions, and are not intentionally enriched in any particular species of nanotube. As a result, only a small fraction of SWNTs are resonant with any given excitation wavelength. Typically, we observe small numbers (usually 5 or less) of RBMs in the spectra and the number varies from spot to spot. While this is not a rigorous measurement of the fraction, density, or number of SWNTs, it is a measure of the number of SWNTs that are resonant with the excitation wavelength. (Histograms of the observed peaks are available in the Supplementary material.) We find that this resonant RBM density is an excellent metric for comparing samples.

The RBM results (plotted vs $1/k_B T$ Fig. 4a) are consistent with [33] in that more RBMs are observed around 850 °C than at lower T. For all $T > 700$ °C RBMs were detected, with N peaking at ~5 near T_c. At all T, RBMs were widely distributed in the range 180–230 cm^{-1} (corresponding to diameters 1.1–1.4 nm where ω [cm^{-1}] $= 248/d$ [nm] [35]). However, above T_c one narrow diameter (~1 nm) mode at 260 cm^{-1} was regularly detected. Surprisingly, N showed characteristic energies (-0.55 ± 0.1 eV and 2.2 ± 0.4 eV above and below T_c, respectively) peaking near T_c. This implies that N is directly connected to the chemical kinetics of nanotube growth. The physical origin of this connection is still unclear.

The G band intensity I_G, which represents the amount of carbon in graphitic form, (plotted vs $1/k_B T$ in Fig. 4b) increased significantly with T with a characteristic energy of 1.5 ± 0.3 eV below

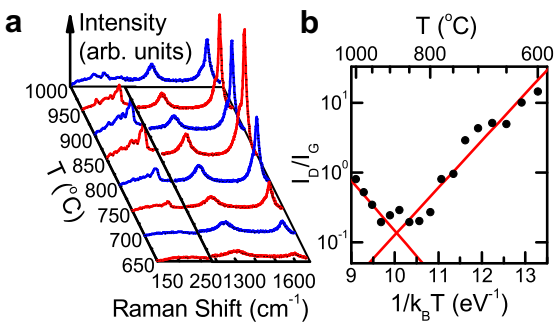

Fig. 3. (a) Raman spectra in RBM and D/G regions for various growth temperatures T. (b) Plot of D/G ratio I_D/I_G vs $1/k_B T$. Solid lines are linear fits.

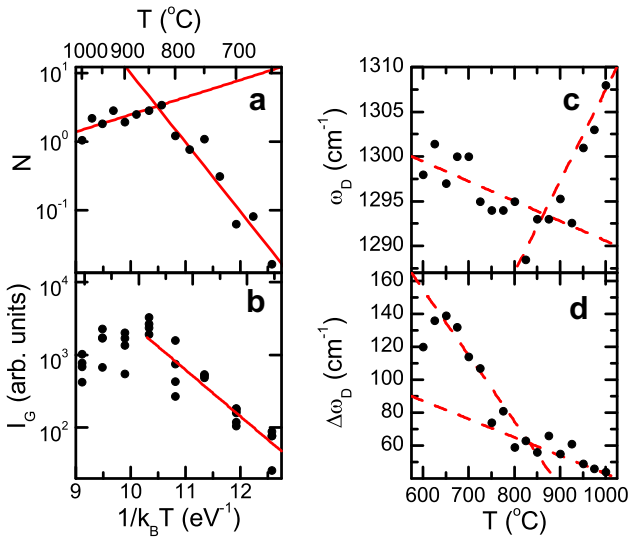

Fig. 4. Plots (vs $1/k_B T$) of (a) average number of RBMs per spot N and (b) G band integrated intensity I_G. (c) Center of D band ω_D and (d) width (FWHM) of D band $\Delta\omega_D$ determined by Lorentzian fits as a function of T. (a) and (b) show characteristic energies. All show critical temperature. Solid lines are linear fits, dashed lines are to guide the eye.

T_c, peaking near T_c before decreasing again. There is too much scatter in the data to determine if there is a characteristic energy above T_c. The D band intensity remained relatively uniform, but it showed more subtle variations in other features.

Fig. 4c shows that the position of the D band ω_D (as a function of T), as determined by Lorentzian fits [36], first decreases and then increases rapidly above T_c. Shifts in ω_D have been attributed to a change in the nanotube diameter [36,37]. For a collection of nanotubes, ω_D is related to the average nanotube diameter [36]. Changes in nanotube diameter have in turn been linked to changes in T [38] and source gas concentration [39].

Fig. 4d shows that the full width at half maximum (FWHM) of the D band $\Delta\omega_D$ (as a function of T) decreases rapidly until T_c, above which it decreases more slowly. We note that while the $\Delta\omega_D$ decreases, I_D/I_G and ω_D increase. This is a more complicated evolution than the overly simple view that more defects leads to a broader, higher D band peak. It is possible that above T_c, a narrower, higher D band corresponds to more of one specific kind of defect.

Below T_c, nanotube growth is slow and the supply of carbon is likely more than sufficient. We speculate that defects may be generated due to overfeeding at low T. Our data (specifically the 1.1 eV activation energy barrier to growth) appears consistent with poor transport of carbon, a commonly proposed limiting mechanism [6,22,23,28,40–42]. As T rises to T_c, β increases more than tenfold and we speculate that the supply of carbon may become insufficient to sustain such high growth rates [43] and defects are increasingly produced as T rises. At T_c, defects are minimized and, in this sense, the growth is optimized. We suppose that the system is then also optimally fed.

We made a preliminary investigation of the effect of feeding by diluting the ethanol/carrier gas mixture and performing *ex situ* Raman spectroscopy of the D and G bands on the resultant forests using a custom built Raman imaging system (described in detail in Ref. [44]) and 532 nm excitation. Below T_c, diluting the ethanol reduced I_D/I_G, consistent with [33]. When diluted to 10% of the initial concentration at 750 °C, I_D/I_G fell from ~1.1 to ~0.4. We conclude that below T_c the system is strongly overfed, consistent with the kinetic data. Above T_c, diluting the ethanol still reduced I_D/I_G, but only marginally (from ~0.3 to ~0.2 at 950 °C). This is contrary to the underfeeding suggested by the slight increase in I_D/I_G with T and decrease in N with T. The slight increase in I_D/I_G with concentration allows us to conclude only that the system is less sensitive to feeding at high T.

4. Conclusion

In summary, there are several important findings: (1) β plateaus above a critical temperature T_c. (2) τ shows the same critical temperature and is connected to β. (3) The D/G ratio also shows the same critical temperature and is also connected to β. (4) Other Raman features show the same critical temperature. (5) β, τ, β/τ, I_D/I_G and N all have the same functional form ($\ln Y \propto 1/k_B T$) where the constant of proportionality is some characteristic energy that was measured for each quantity. For β and τ, these energies may be interpreted as activation energies for some chemical process. (6) Here, we rule out diffusion through the forest as a limiting factor of the growth rate. Future models should provide a detailed explanation of the growth kinetics, the critical point, the Raman spectral features, and the connections between them.

The value of *in situ* measurements of carbon nanotube growth kinetics is clear. Furthermore, a wealth of data about the growth kinetics is imprinted on *ex situ* Raman spectral features. We expect similar experiments in the near future to yield even greater insights and play an important role in developing more complete models of nanotube synthesis.

Acknowledgements

We are grateful for preliminary work by J. Bond, assistance with the Raman system by L. Tay, the continuing support of P. Marshall, and the assistance of H. Tran, P. Chow-Chong, M. Denhoff, K. Kaminska, J. Fraser, and D.G. Austing. P.V. was supported by OGS, NSERC, and NRC-GSSSP. P.V. and P.F. were supported by an NSERC Discovery Grant. P.F. is grateful for the support of JST-CREST.

Appendix A. Supplementary material

Supplementary data associated with this article can be found, in the online version, at doi:10.1016/j.cplett.2008.12.095.

References

[1] E. Joselevich, H. Dai, J. Liu, K. Hata, A.H. Windle, in: A. Jorio, G. Dresselhaus, M.S. Dresselhaus (Eds.), Ch. Carbon Nanotube Synthesis and Organization, Topics in Applied Physics, vol. 111, Springer-Verlag, 2008, p. 101.
[2] G. Eres, A.A. Puretzky, D.B. Geohegan, H. Cui, Appl. Phys. Lett. 84 (2004) 1759.
[3] D.N. Futaba, K. Hata, T. Yamada, K. Mizuno, M. Yumura, S. Iijima, Phys. Rev. Lett. 95 (2005) 056104.
[4] A.A. Puretzky, D.B. Geohegan, S. Jesse, I.N. Ivanov, G. Eres, Appl. Phys. A 81 (2005) 223.
[5] A.A. Puretzky, G. Eres, C.M. Rouleau, I.N. Ivanov, D.B. Geohegan, Nanotechnology 19 (2008) 055605.
[6] S.K. Pal et al., Nanotechnology 19 (2008) 045610.
[7] E. Einarsson, Y. Murakami, M. Kadowaki, S. Maruyama, Carbon 46 (2008) 923.
[8] E. Einarsson et al., J. Nanosci. Nanotech. 8 (2008) 6093.
[9] Z.F. Ren, Z.P. Huang, J.W. Xu, J.H. Wang, P. Bush, M.P. Siegal, P.N. Provencio, Science 282 (1998) 1105.
[10] S. Fan, M.G. Chapline, N.R. Franklin, T.W. Tombler, A.M. Cassell, H. Dai, Science 283 (1999) 512.
[11] Y. Murakami, S. Chiashi, Y. Miyauchi, M. Hu, M. Ogura, T. Okubo, S. Maruyama, Chem. Phys. Lett. 385 (2004) 298.
[12] K. Hata, D.N. Futaba, K. Mizuno, T. Namai, M. Yumura, S. Iijima, Science 306 (2004) 1362.
[13] G.F. Zhong, T. Iwasaki, K. Honda, Y. Furukawa, I. Ohdomari, H. Kawarada, Chem. Vap. Dep. 11 (2005) 127.
[14] K. Kaminska, J. Lefebvre, D.G. Austing, P. Finnie, Nanotechnology 18 (2007) 65707.
[15] I. Gunjishima, T. Inoue, A. Okamoto, Appl. Phys. Lett. 91 (2007) 193102.
[16] P. Finnie, J. Bardwell, I. Tsandev, M. Tomlinson, M. Beaulieu, J. Fraser, J. Lefebvre, J. Vac. Sci. Technol. 22 (2004) 747.
[17] P. Finnie, A. Li-Pook-Than, J. Lefebvre, D.G. Austing, Carbon 44 (2006) 3199.
[18] S. Chiashi, Y. Murakami, Y. Miyauchi, S. Maruyama, Chem. Phys. Lett. 386 (2004) 89.
[19] J. Kong, A.M. Cassell, H. Dai, Chem. Phys. Lett. 292 (1998) 567.
[20] S. Maruyama, R. Kojima, Y. Miyauchi, S. Chiashi, M. Kohno, Chem. Phys. Lett. 360 (2002) 229.
[21] C. Ducati, I. Alexandrou, M. Chhowalla, G.A.J. Amaratunga, J. Robertson, J. Appl. Phys. 92 (2002) 3299.
[22] Y.T. Lee, N.S. Kim, J. Park, J.B. Han, Y.S. Choi, H. Ryu, H.J. Lee, Chem. Phys. Lett. 372 (2003) 853.
[23] K.-E. Kim, K.-J. Kim, W.S. Jung, S.Y. Bae, J. Park, J. Choi, J. Choo, Chem. Phys. Lett. 401 (2005) 459.
[24] M. Picher, V. Jourdain, E. Anglaret, Growth regimes of CCVD-grown SWCNTs determined by in situ Raman spectroscopy, poster B 85, Ninth International Conference on the Science and Applications of Nanotubes, NT08 (2008).
[25] M.J. Bronikowski, J. Phys. Chem. C 111 (2007) 17705.
[26] S. Iijima, private communication (May 2008).
[27] C. Singh, M.S.P. Shaffer, A.H. Windle, Carbon 41 (2003) 359.
[28] O.A. Louchev, T. Laude, Y. Sato, H. Kanda, J. Chem. Phys. 118 (2003) 7622.
[29] G. Zhong, T. Iwasaki, J. Robertson, H. Kawarada, J. Phys. Chem. B 111 (2007) 1907.
[30] R. Xiang et al., J. Phys. Chem. C 112 (2008) 4892.
[31] H. Cui, G. Eres, J.Y. Howe, A. Puretzky, M. Varela, D.B. Geohegan, D.H. Lowndes, Chem. Phys. Lett. 374 (2003) 222.
[32] G. Eres, A.A. Kinkhabwala, H. Cui, D.B. Geohegan, A.A. Puretzky, D.H. Lowndes, J. Phys. Chem. B 109 (2005) 16684.
[33] H.E. Unalan, M. Chhowalla, Nanotechnology 16 (2005) 2153.
[34] J. Bond, J. Lefebvre, D.G. Austing, L. Tay, P. Finnie, Nanotechnology 18 (2007) 135603.
[35] A. Jorio et al., Phys. Rev. Lett. 86 (2001) 1118.
[36] A. Jorio, M.A. Pimenta, A.G. Souza Filho, R. Saito, G. Dresselhaus, M.S. Dresselhaus, New J. Phys. 5 (2003) 139.
[37] A.G. Souza Filho et al., Phys. Rev. B 67 (2003) 035427.

[38] Y. Yao, Q. Li, J. Zhang, R. Liu, L. Jiao, Y.T. Zhu, Z. Liu, Nat. Mater. 6 (2007) 283.
[39] C. Lu, J. Liu, J. Phys. Chem. B 110 (2006) 20254.
[40] S. Helveg et al., Nature 427 (2004) 426.
[41] S. Hofmann, G. Csányi, A.C. Ferrari, M.C. Payne, J. Robertson, Phys. Rev. Lett. 95 (2005) 036101.
[42] H. Kanzow, A. Schmalz, A. Ding, Chem. Phys. Lett. 295 (1998) 525.
[43] L. Ci et al., Chem. Phys. Lett. 349 (2001) 191.
[44] K. Kaminska, J. Lefebvre, D.G. Austing, P. Finnie, Phys. Rev. B 73 (2006) 235410.